New York, 1990), pp. 170–177.
16. At model section 200, the algorithmically calculated gain of the dependent source feeding into the upper line was manually assigned the same value as section 199. This was about a 5.8% variation from the originally assigned gain for that section.
17. D. Kemp, *J. Acoust. Soc. Am.* **64**, 1386 (1978).
18. J. Wilson, *Hear. Res.* **2**, 233 (1980).
19. D. Shine, thesis, Boston University (1991).
20. I removed section 99 and used a voltage source to drive it. Longitudinal inductors were not present.
21. The single-section active 3-dB bandwidth is ≈2000 Hz, about twice that of every other 3-dB bandwidth.
22. I confirmed the hypothesized velocity match region by running the model with $M_2(x) = \infty$ in the lower line and comparing phase-versus-frequency results (*26*) for this configuration and for the lower line disconnected from the upper line. The full model in the local-feedback configuration produces passive-looking, not elevated, peaks on the upper line. This behavior also demonstrates the distributed nature of the amplification.
23. Impedance is $V(x)/I(x)$. Power is $V(x)I(x)$. See Fig. 2.
24. E. de Boer, *J. Acoust. Soc. Am.* **73**, 567 (1983).
25. A. Cody, *Hear. Res.* **62**, 166 (1992); A. Hubbard, D. Gonzales, D. Mountain, Abstracts of the 16th Midwinter Meeting of the Association for Research in Otolaryngology, accepted for publication. See also J. Allen and P. Fahey [*J. Acoust. Soc. Am.* **92**, 178 (1992)], who uses experimental data to show there is little or no cochlear amplification.
26. Group delay is (minus) the slope of the phase-versus-frequency curve.
27. One must more carefully chose parameters to match specific data.
28. A. Cody, D. Gonzales, P. Jung, D. Mountain, H. Voigt, and S. Xue aided the preparation of this manuscript. Support provided by the Office of Naval Research and NIH.

26 May 1992; accepted 7 October 1992

Vapor Pressures of Solid Hydrates of Nitric Acid: Implications for Polar Stratospheric Clouds

Douglas R. Worsnop,* Lewis E. Fox, Mark S. Zahniser, Steven C. Wofsy

Thermodynamic data are presented for hydrates of nitric acid: $HNO_3 \cdot H_2O$, $HNO_3 \cdot 2H_2O$, $HNO_3 \cdot 3H_2O$, and a higher hydrate. Laboratory data indicate that nucleation and persistence of metastable $HNO_3 \cdot 2H_2O$ may be favored in polar stratospheric clouds over the slightly more stable $HNO_3 \cdot 3H_2O$. Atmospheric observations indicate that some polar stratospheric clouds may be composed of $HNO_3 \cdot 2H_2O$ and $HNO_3 \cdot 3H_2O$. Vapor transfer from $HNO_3 \cdot 2H_2O$ to $HNO_3 \cdot 3H_2O$ could be a key step in the sedimentation of HNO_3, which plays an important role in the depletion of polar ozone.

Polar stratospheric clouds (PSCs) (*1–3*) play two essential roles in perturbing the chemistry of stratospheric O_3 during winter: (i) PSCs provide reactive surfaces that convert inorganic chlorine to reactive form and nitrogen oxides to HNO_3 (*4, 5*) and (ii) sedimentation of PSC particles containing HNO_3 leads to irreversible removal of nitrogen oxides ("denitrification"). The efficiency of denitrification is crucial for polar O_3 depletion. If substantial gaseous HNO_3 is present in late winter, it photolyzes to release NO_x radicals, which combine with ClO, halting O_3 destruction (*4, 6*). Denitrification is nearly complete over Antarctica and large O_3 losses are observed (*7*); denitrification is sporadic in the Arctic (*8*) and O_3 losses are much smaller.

Type I PSCs condense at temperatures 2 to 4 K above the frost point of water ice (*1*). Solid hydrates of HNO_3 have been proposed as the major components of type I PSCs (*2, 3*), and nitrogen oxides have been observed in PSC particles (*7, 8*). The principal phase is usually assumed to be nitric acid trihydrate ($HNO_3 \cdot 3H_2O$) (*2, 3, 6*), the most stable hydrate under stratospheric conditions (*9*). However, careful analysis of field observations of total nitrogen oxides and aerosol particles (*10*) indicates that PSCs form at temperatures 2 to 4 K colder than the equilibrium temperature for $HNO_3 \cdot 3H_2O$. Partial pressures of HNO_3 in PSCs (*11*) were observed to exceed equilibrium with $HNO_3 \cdot 3H_2O$; this led Arnold (*12*) to argue that the condensed phase could be a supercooled liquid (*13*) rather than $HNO_3 \cdot 3H_2O$.

This report presents the results of laboratory studies of hydrates of HNO_3 under conditions of temperature and gas-phase HNO_3 and H_2O concentrations approaching those found in the stratosphere. We show that nitric acid dihydrate ($HNO_3 \cdot 2H_2O$) is only slightly less stable than $HNO_3 \cdot 3H_2O$ and is a likely metastable component of type I PSCs. Thin films of $HNO_3 \cdot 2H_2O$ have been reported (*14*), but no thermodynamic information has been available. We also identify a higher hydrate, possibly $HNO_3 \cdot 10H_2O$ (*15, 16*).

Vapor pressures of HNO_3 and H_2O were measured by infrared tunable diode laser absorption spectroscopy with a multiple-pass Herriott cell (40 passes, 50 cm per pass; 7.6-cm-diameter gold-coated mirrors) mounted vertically in a 12-liter vacuum chamber constructed of gold-plated stainless steel and glass coated with $C_6F_{13}CH_2CH_2Si(OC_2H_5)_3$ (Petrarch Systems) (see Fig. 1). We determined partial pressures p_{H_2O} and p_{HNO_3} by fitting Gaussian line profiles for 12 HNO_3 lines and 1 H_2O line between 1339.97 and 1340.18 cm^{-1}, with line strengths derived from recent measurements (*17*). Detection limits were $\sim 10^{-7}$ torr for HNO_3 and $[HNO_3]/50$ for H_2O, limited by interference fringes for HNO_3 and by a weak HNO_3 feature for H_2O.

We regulated sample temperatures between 190 and 230 K by allowing cold nitrogen gas to flow onto a brass button epoxied to the cell exterior 20 cm below the detection region. We condensed solid phases on the glass surface above the button by cooling mixtures of gaseous H_2O and HNO_3 or by adding gaseous H_2O or HNO_3 to a cold sample. The thickness of the condensed layer varied between 5 and 50 μm, estimated from the amount of gas-phase H_2O and HNO_3 that condensed. The button temperature could be regulated with a precision of ±0.2 K [accuracy approximately ±0.4 K (*18*)], as confirmed by comparing p_{H_2O} to literature values (*19*). The cell temperature above the cold point was set to 273 K for most experiments. Heating or cooling the Herriott cell between 240 and 295 K had no measurable effect on vapor pressures, indicating negligible influence of gases adsorbed on chamber walls.

The chamber was sealed under vacuum during the experiments, except during the addition of H_2O or HNO_3 through the manifold. Mixtures placed into the cell typically did not match the stoichiometry of a crystalline hydrate; consequently, two or three solid phases condensed on the cold spot in equilibrium with a vapor phase ("triple" or "quadruple" points, respectively). Partial pressures (p_{HNO_3} and p_{H_2O}) equilibrated with a surface layer of a single crystalline phase when vapor was added to the chamber. For example, in an experiment in which $HNO_3 \cdot 3H_2O$ and ice were condensed above the cold button, a surface layer of $HNO_3 \cdot 3H_2O$ alone was formed on addition of HNO_3 at pressures of 10^{-4} to 2×10^{-2} torr. Vapor pressures in the cell equilibrated with this layer, as demonstrated by the variation of p_{HNO_3} and p_{H_2O} according to the Gibbs-Duhem equation

$$d(\ln p_{HNO_3})/d(\ln p_{H_2O}) = -n \qquad (1)$$

where n is the H_2O/HNO_3 ratio in the solid phase. Over a period of many minutes, water diffused from the underlying solid, driving p_{HNO_3} and p_{H_2O} back to the triple point according to Eq. 1 (with $n = 3$). This behav-

D. R. Worsnop and M. S. Zahniser, Center for Chemical and Environmental Physics, Aerodyne Research, Inc., Billerica, MA 01821.
L. E. Fox and S. C. Wofsy, Division of Applied Sciences, Harvard University, Cambridge, MA 02138.

*To whom correspondence should be addressed.

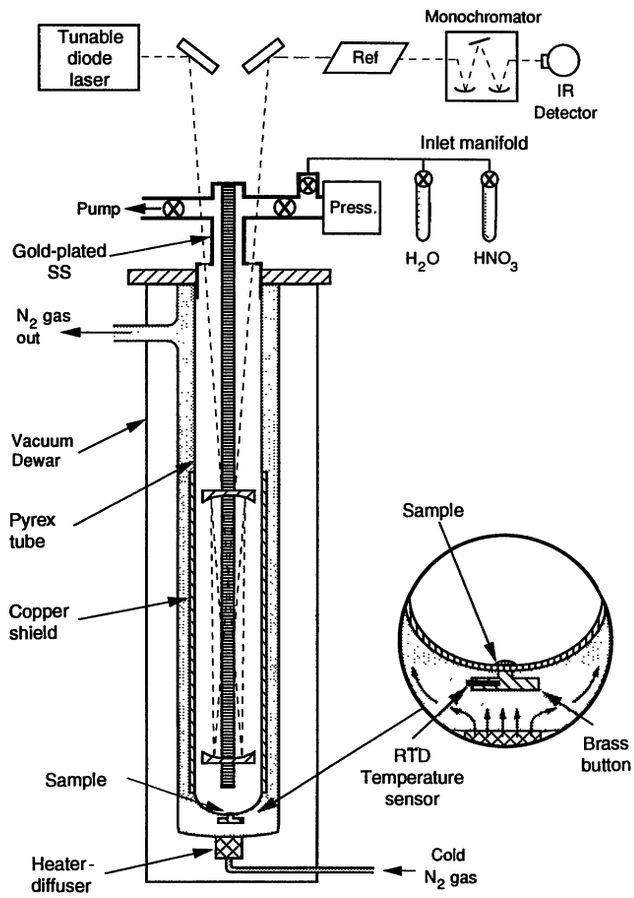

Fig. 1. Experimental apparatus; SS, stainless steel. Gas-phase HNO_3 and H_2O mixtures are condensed on the coldest point at the bottom of the Pyrex chamber. A thermal gradient, between the cold spot above the brass button and the warmer side walls heated by the copper shield, confines the size of the condensed sample to ≤1 cm diameter (inset). Gas-phase equilibrium vapor pressures are measured by infrared (IR) laser absorption using multiple pass mirrors.

ior provided unambiguous identification of $HNO_3 \cdot 3H_2O$ as the surface phase. Surface layers of $HNO_3 \cdot H_2O$, $HNO_3 \cdot 2H_2O$, and $HNO_3 \cdot 3H_2O$ were readily identified in this way, concurrent with determination of fugacities for these phases.

Vapor pressure data for HNO_3 hydrates (n = 1, 2, and 3) are summarized in Fig. 2, which shows all measurements for which the surface layer and gas phase were equilibrated ($\Delta p_i/p_i < 0.2$ in 5 min). Results are summarized in Fig. 3 as a plot of the natural logarithm of the equilibrium constant, K_n, versus $1/T$, where

$$K_n = p_{HNO_3} (p_{H_2O})^n \qquad (2)$$

for (n = 1, 2, and 3). Standard enthalpy ($\Delta H°/R$) and entropy ($\Delta S°/R$) values (inset in Fig. 3) for the vapor- to solid-phase transitions are obtained from the slopes and intercepts of the linear least squares fits. Our values for K_3 agree closely with the data of Hanson and Mauersberger (*9, 20*) (see Fig. 3), indicating that, as they concluded, $HNO_3 \cdot 3H_2O$ is the most stable hydrate in the stratosphere. This hydrate is stable at temperatures 4 to 6 K above the ice frost point under stratospheric conditions. The quadruple point for vapor, $HNO_3 \cdot H_2O$, $HNO_3 \cdot 2H_2O$, and $HNO_3 \cdot 3H_2O$ was observed at about 212 K (there are no degrees of freedom at this point). In experiments at 190.8 and 196.4 K, and with p_{HNO_3} a factor of 10 higher than found in the stratosphere, $HNO_3 \cdot 2H_2O$ was the most stable phase.

Metastable hydrates of HNO_3 formed readily and persisted for as long as several days (Fig. 4A). Initial condensation at the quadruple point (212 K) formed $HNO_3 \cdot H_2O$ and $HNO_3 \cdot 2H_2O$. Repeated additions of H_2O produced metastable $HNO_3 \cdot 2H_2O$ (the blue n = 2 line) with no sign of the more stable $HNO_3 \cdot 3H_2O$. In separate experiments at this temperature, after addition of excess H_2O formed $HNO_3 \cdot 3H_2O$, repeated additions of HNO_3 produced vapor pressures lying on the (red) n = 3 line in Fig. 4A, indicative of stable $HNO_3 \cdot 3H_2O$.

Nucleation of $HNO_3 \cdot 3H_2O$ appeared to

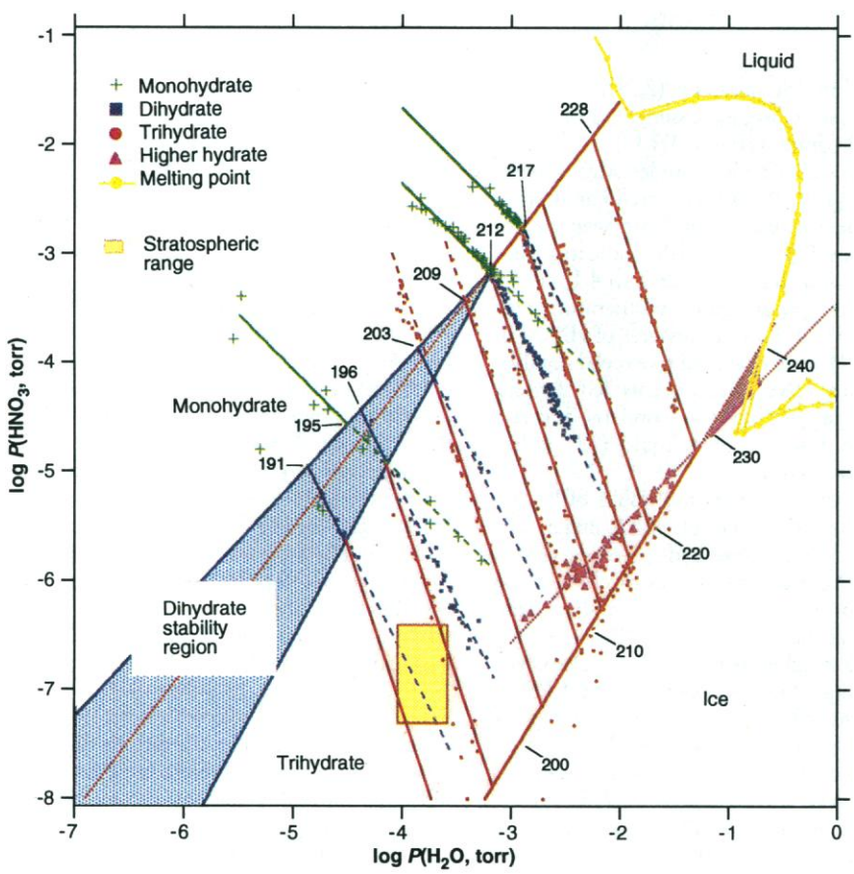

Fig. 2. Nitric acid–water phase diagram [log p_{HNO_3}(torr) versus log p_{H_2O} (torr)], with data for each phase-coded by color and symbol as shown in the key. Color-coded lines with slopes −1, −2, and −3 represent the Gibbs-Duhem relation (Eq. 1) at the specified temperature for the corresponding value of n. Solid and dashed lines denote stable and metastable phases, respectively. Lines with positive slopes delineate phase boundaries between ice, $HNO_3 \cdot 3H_2O$, $HNO_3 \cdot 2H_2O$, and $HNO_3 \cdot H_2O$ for stable (solid lines) and metastable (dotted lines) phases calculated from the equilibrium constants determined in Fig. 3. A higher hydrate was observed in coexistence with ice as shown (magenta). The shaded areas show regions of stability for $HNO_3 \cdot 2H_2O$ and the higher hydrate (blue and magenta, respectively). The melting point curve is interpolated based on the use of two sets of data from Pickering (*15, 16*).

be triggered when the saturation ratio, $S_{HNO_3 \cdot 3H_2O} = p_{HNO_3}(p_{H_2O})^3/K_3$, was raised above 8, as illustrated in Fig. 4B. Here we show data for the addition of HNO_3 to a sample of $HNO_3 \cdot 3H_2O$ and ice. Initially $HNO_3 \cdot H_2O$ was formed, followed by $HNO_3 \cdot 2H_2O$ (5 to 30 min), as indicated by successive points lying on the $n = 2$ line. When $S_{HNO_3 \cdot 3H_2O}$ reached 6 to 10, $HNO_3 \cdot 3H_2O$ suddenly reappeared. In many experiments, a pause in the time evolution of p_{HNO_3} and p_{H_2O} was observed, for 1 to 20 min, at values consistent with the formation of transient metastable phases. Supersaturation of H_2O relative to ice was never observed, nor did we observe the coexistence of ice with (metastable) $HNO_3 \cdot 2H_2O$.

Condensation of gas mixtures with p_{H_2O}/p_{HNO_3} ratios initially between 20 to 100, at temperatures >205 K, typically produced a solid for which p_{H_2O} equilibrated with ice, but p_{HNO_3} was elevated relative to $HNO_3 \cdot 3H_2O$ by as much as $S_{HNO_3 \cdot 3H_2O} = 8$. We infer from this behavior that a metastable higher hydrate of HNO_3 was formed, along with ice, on the cold button. Varying the cold button temperature between 203 and 230 K delineated a coexistence boundary between this hydrate and ice (Fig. 2). Supersaturation of HNO_3 vapor relative to $HNO_3 \cdot 3H_2O$ persisted until the temperatures dropped below 203 K, where $S_{HNO_3 \cdot 3H_2O} > 8$. Nucleation of $HNO_3 \cdot 3H_2O$ brought p_{HNO_3} into equilibrium with $HNO_3 \cdot 3H_2O$ at the ice–$HNO_3 \cdot 3H_2O$–vapor triple point. The higher hydrate could not be reformed unless the solid was completely evaporated. Extrapolation of the phase boundary to the liquidus suggests a eutectic (*15*) involving ice plus a higher hydrate. The hydrate composition is possibly $HNO_3 \cdot 10H_2O$, as suggested in the original studies by Pickering (*15, 16*).

The tendency to nucleate persistent metastable phases may indicate a relatively high free-energy barrier for nucleation of $HNO_3 \cdot 3H_2O$, compared to other crystalline hydrates. Metastable phases are favored in a variety of condensation phenomena, for example, for formation of supercooled water droplets (*21*) or metallic alloys (*22*). This behavior reflects a tendency for the most stable phases to be more highly ordered, with correspondingly higher surface free energies (*22*). If formation of metastable $HNO_3 \cdot 2H_2O$ is favored over the formation of $HNO_3 \cdot 3H_2O$ in the stratosphere, as observed under laboratory conditions, then p_{HNO_3} in some type I PSCs would be maintained above its equilibrium value with $HNO_3 \cdot 3H_2O$. The saturation ratio $S_{HNO_3 \cdot 3H_2O}$ would be less than 8, the value that triggered nucleation of $HNO_3 \cdot 3H_2O$ in the laboratory, until temperatures dropped to the frost point ($S_{HNO_3 \cdot 3H_2O} \approx 9$, $T = 185$ to 192 K).

Several observations support a role for $HNO_3 \cdot 2H_2O$ in PSCs. PSCs often appear at temperatures 2 to 4 K below the $HNO_3 \cdot 3H_2O$ threshold (*7, 8*), cold enough to form $HNO_3 \cdot 2H_2O$ but not cold enough to produce the saturation ratio $S_{HNO_3 \cdot 3H_2O} > 8$ required for $HNO_3 \cdot 3H_2O$ formation in the laboratory. The measurements of p_{HNO_3} by Arnold and co-workers (*11*) in PSCs over Kiruna, Sweden, on 31 January 1989 were consistent with two regions of $HNO_3 \cdot 2H_2O$, separated by a region of $HNO_3 \cdot 3H_2O$ in a cold zone where $S_{HNO_3 \cdot 3H_2O}$ would have exceeded 8. We believe that $HNO_3 \cdot 2H_2O$ could have been the metastable phase sought by Arnold (*12*) to explain some cases for which he observed $S_{HNO_3 \cdot 3H_2O} > 1$. The "higher" hydrate is a less likely candidate because it would form only with $S_{HNO_3 \cdot 3H_2O} > 10$ at a temperature below 200 K.

Our results confirm earlier work (*2–9*) indicating that hydrates of HNO_3 are probable components of type I PSCs and that $HNO_3 \cdot 3H_2O$ is the most stable phase in the stratosphere. We showed that $HNO_3 \cdot 2H_2O$ is only slightly less stable; it is formed

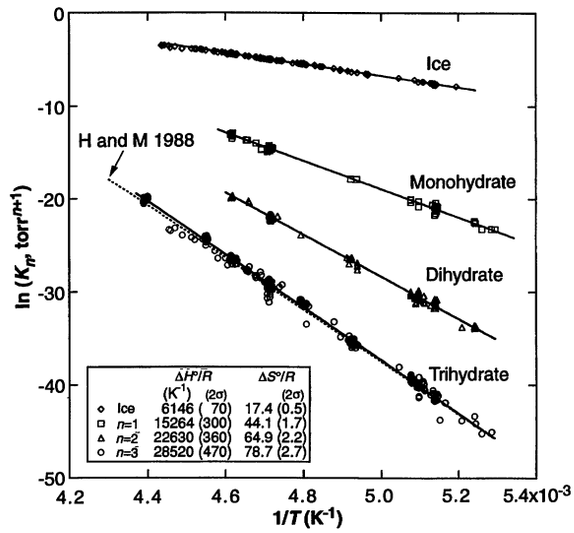

Fig. 3. Equilibrium constants K_n from Eq. 2 for ice and $HNO_3 \cdot nH_2O$ ($n = 1$, 2, and 3) from the data in Fig. 2. Units are torr for ice and torr^{n+1} for the hydrates. Enthalpy and entropy values are obtained from the slopes ($\Delta H^\circ/R = -A$) and intercepts [$\Delta S^\circ/R = B - (n + 1)\ln(760)$] of the least squares fit to the form $\ln K_n = A/T + B$. Ice data points are used to calibrate the sample temperature (*18*) based on the use of literature values for ΔH° and ΔS° (*21*). Statistical uncertainties (2σ) from the least squares fit for $\Delta H^\circ/R$ and $\Delta S^\circ/R$ are listed (*18*). Previous results for $HNO_3 \cdot 3H_2O$ (*9, 20*) are shown for comparison.

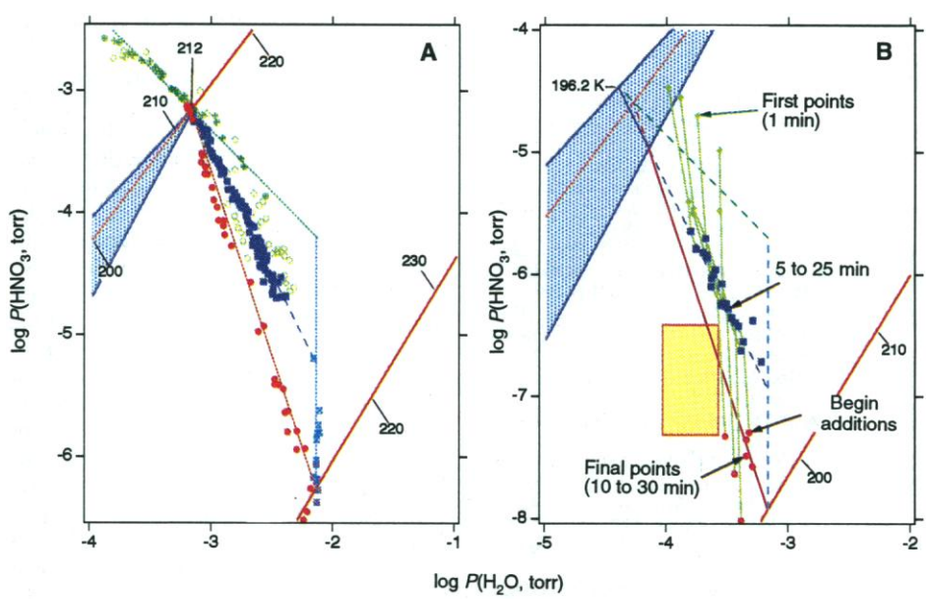

Fig. 4. Time evolution of p_{HNO_3} and p_{H_2O} equilibration with surface layers formed by gas condensation on a solid sample, with symbols as in Fig. 2. (**A**) Condensation of $HNO_3 \cdot 2H_2O$ and $HNO_3 \cdot H_2O$ at the quadruple point followed by water vapor additions. Only $HNO_3 \cdot 2H_2O$ was formed (the saturation ratio $S_{HNO_3 \cdot 3H_2O}$ was always less than 8). In separate experiments at the same temperature, with excess H_2O in the sample, $HNO_3 \cdot 3H_2O$ was formed. Repeated additions of HNO_3 produced the $n = 3$ line (red) indicative of a surface layer of $HNO_3 \cdot 3H_2O$. (**B**) Results of four experiments in which $HNO_3 \cdot H_2O$ and $HNO_3 \cdot 2H_2O$ were formed over a $HNO_3 \cdot 3H_2O$ substrate by the addition of HNO_3 at 196.2 K. Metastable $HNO_3 \cdot H_2O$ was observed at 1 min; then $HNO_3 \cdot 2H_2O$ formed, persisting for 5 to 25 min before the transition to $HNO_3 \cdot 3H_2O$ at $S_{HNO_3 \cdot 3H_2O} = 6$ to 10. The color-code is as in Fig. 2.

readily under milder condensation conditions than $HNO_3 \cdot 3H_2O$, and it is therefore a probable component of PSCs.

The HNO_3 vapor pressure in a cloud of $HNO_3 \cdot 2H_2O$ would be supersaturated relative to $HNO_3 \cdot 3H_2O$, but $S_{HNO_3 \cdot 3H_2O}$ does not exceed the value needed for nucleation (~8) until ambient temperatures fall close to the ice frost point (where $S_{HNO_3 \cdot 3H_2O} \sim 9$). We infer that nucleation of $HNO_3 \cdot 3H_2O$ may coincide with the formation of ice clouds (type II PSCs). This sequence would be consistent with the idea (*23*) that falling ice particles could play a key role in denitrification: excess HNO_3 vapor, present in a cloud of metastable $HNO_3 \cdot 2H_2O$, would be available for rapid, efficient transfer to any $HNO_3 \cdot 3H_2O$ on the surface of a falling ice particle.

Temperatures below the ice point are much more prevalent in Antarctica than in the Arctic. The mechanism proposed here would help explain (*23, 24*) observed denitrification in both polar regions, (*7, 8*) and may contribute to the associated north-south asymmetry in the severity of O_3 loss. Thus, understanding the complex thermodynamics of hydrates of HNO_3 may be crucial to understanding the mechanisms for severe depletion of polar O_3.

REFERENCES AND NOTES

1. M. P. McCormick, H. M. Steele, P. Hamill, W. B. Chu, T. J. Swissler, *J. Atmos. Sci.* **39**, 1387 (1982); H. M. Steele, P. Hamill, M. P. McCormick, T. J. Swissler, *ibid.* **40**, 2055 (1983).
2. P. J. Crutzen and F. Arnold, *Nature* **324**, 651 (1986).
3. O. B. Toon, P. Hamill, R. P. Turco, J. Pinto, *Geophys. Res. Lett.* **13**, 1284 (1986).
4. S. Solomon *et al.*, *Nature* **321**, 755 (1986); M. B. McElroy *et al.*, *ibid.*, p. 759.
5. M. J. Molina *et al.*, *Science* **238**, 1253 (1987); M. A. Tolbert *et al.*, *ibid.*, p. 1258; M.-T. Leu, *Geophys. Res. Lett.* **15**, 17 (1988); *ibid.*, p. 851; M. A. Tolbert *et al.*, *Science* **240**, 1018 (1988).
6. M. B. McElroy, R. J. Salawitch, S. C. Wofsy, *Geophys. Res. Lett.* **13**, 1296 (1986); R. J. Salawitch, S. C. Wofsy, M. B. McElroy, *ibid.* **15**, 871 (1988).
7. D. W. Fahey *et al.*, *J. Geophys. Res.* **94**, 11299 (1989); D. W. Fahey *et al.*, *Nature* **344**, 321 (1990).
8. S. R. Kawa *et al.*, *Geophys. Res. Lett.* **17**, 485 (1990); *J. Geophys. Res.* **97**, 7925 (1992); J. E. Dye *et al.*, *ibid.*, p. 8015.
9. D. Hanson and K. Mauersberger, *Geophys. Res. Lett.* **15**, 855 (1988).
10. J. E. Dye *et al.*, *ibid.* **17**, 413 (1990).
11. H. Schlager and F. Arnold, *ibid.*, p. 433; Y. Kondo *et al.*, *ibid.*, p. 437; H. Schlager, F. Arnold, D. Hofmann, T. Deshler, *ibid.*, p. 1275.
12. F. Arnold, *Ber. Bunsenges. Phys. Chem.* **96**, 339 (1992).
13. D. R. Hanson, *Geophys. Res. Lett.* **17**, 421 (1990).
14. G. Ritzhaupt and J. P. Devlin, *J. Phys. Chem.* **95**, 90 (1991); M. A. Tolbert and A. M. Middlebrook, *J. Geophys. Res.* **95**, 22423 (1990); B. G. Koehler *et al.*, *ibid.* **97**, 8065 (1992).
15. S. U. Pickering, *J. Chem. Soc.* **63**, 436 (1893).
16. Pickering (*15*) speculated on the existence of a hexadecahydrate of HNO_3; our extrapolation of vapor pressure data to his freezing-point curve is more consistent with $HNO_3 \cdot 10H_2O$.
17. Nitric acid and water vapor concentrations were retrieved with line parameters (positions, strengths, and lower state energies) from the HITRAN database [L. S. Rothman *et al.*, *J. Quant. Spectrosc. Radiat. Transfer* **48**, 469 (1992)]. Nitric acid line strengths were multiplied by 1.14 to obtain agreement with the absolute measurements of R. D. May and C. R. Webster [*ibid.* **38**, 5 (1987)].
18. We calibrated the temperature scale of Fig. 3 by fitting the H_2O vapor pressures of ice-containing samples ($HNO_3 \cdot 3H_2O$ and higher hydrate triple points) to known ice vapor pressures (*21*). This accounted for both the temperature difference of the cold spot over the cold button (see inset in Fig. 1) and the absolute calibration of the resistance temperature device (RTD) temperature sensor. This amounted to a ±1 K correction of the RTD reading (precision ±0.2 K) over our experimental temperature range. Statistical deviations in the reproducibility of the H_2O vapor measurement correspond to a ±0.4 K uncertainty in the relative temperature. Statistical uncertainties (2σ) for $\Delta H^\circ/R$ and $\Delta S^\circ/R$ (where R is the gas constant) are listed in Fig. 3. Uncertainties of ~10% and ~20% in the H_2O and HNO_3 line strengths (*17*), respectively, are included in the $\Delta S^\circ/R$ uncertainties.
19. G. Jansco *et al.*, *J. Phys. Chem.* **74**, 2984 (1970).
20. R. H. Smith, *Geophys. Res. Lett.* **17**, 1291 (1990).
21. H. R. Pruppacher and J. D. Klett, *Microphysics of Clouds and Precipitation* (Reidel, Dordrecht, Holland, 1978), p. 714.
22. D. Turnbull, *Metal. Trans. A* **124**, 695 (1981).
23. S. C. Wofsy, R. J. Salawitch, J. H. Yatteau, M. B. McElroy, *Geophys. Res. Lett.* **17**, 449 (1990).
24. R. J. Salawitch *et al.*, *Nature* **339**, 525 (1989).

25. Discussions with M. A. Tolbert, D. Turnbull, O. B. Toon, and C. E. Kolb and the technical expertise of S. Kallelis are gratefully acknowledged. This work was supported by National Science Foundation grant DPP-8813379 to Harvard University and by National Aeronautics and Space Administration grants NASW 4126 and NAS1-19161 to Aerodyne Research, Inc.

13 July 1992; accepted 2 November 1992

Identification of a Whitefly Species by Genomic and Behavioral Studies

Thomas M. Perring,* Arthur D. Cooper, Russell J. Rodriguez, Charles A. Farrar, Tom S. Bellows, Jr.

An introduced whitefly species, responsible for over a half billion dollars in damage to U.S. agricultural production in 1991, is morphologically indistinguishable from *Bemisia tabaci* (Gennadius). However, with the use of polymerase chain reaction–based DNA differentiation tests, allozymic frequency analyses, crossing experiments, and mating behavior studies, the introduced whitefly is found to be a distinct species. Recognition of this new species, the silverleaf whitefly, is critical in the search for management options.

An introduced whitefly had a large impact on the production of many food and fiber crops in the southern United States in 1991 (*1, 2*). Integrated crop management and increased applications of currently available pesticides failed to curb the infestations. The resulting agricultural losses have been estimated at over a half billion dollars (*2*).

Whiteflies of the type referred to as the sweet-potato whitefly, *Bemisia tabaci* (Gennadius) "type A" or "cotton strain," have been present in the United States for approximately 100 years (*3*) without causing losses of the magnitude experienced in 1991. The newly introduced variant that apparently caused the 1991 damage became known as "superbug" (*4*) ("type B" or "poinsettia strain") and, based on morphological similarities with the sweet-potato whitefly, has been thought to be a strain of *B. tabaci* (*5*). Isozyme (*5, 6*) and biological (*7*) studies indicate differences between whiteflies of types A and B. A national plan for research on "*B. tabaci*" has been established (*8*).

The sweet-potato whitefly first was described as *Aleyrodes tabaci* and was isolated from tobacco in Greece (*9*). Since that time, the whitefly has been redescribed in synonymy 22 times and has been recorded from nearly all tropical and subtropical regions (*10–12*). However, the systematics of this group of whiteflies and of the two whiteflies predominant in the United States must be determined because control strategies based on existing knowledge of "*B. tabaci*" (*13*) may not be successful when applied to different species.

Species may be defined as "natural populations that are reproductively isolated from one another and that follow distinct and independent evolutionary paths" (*14*). We used crossing experiments and mating behavior studies to analyze reproductive isolation and genomic studies to elucidate the evolutionary paths followed by the two whitefly types.

All possible crosses among three whitefly populations were performed (Table 1). Two colonies (A1 and A2) were of type A whiteflies, and one colony (B) was of type B whiteflies. To ensure that no mating had occurred prior to placing whiteflies in pairs, leaves with late-instar whitefly nymphs were removed from respective colonies 15 to 18 hours preceeding the experiment; *B. tabaci* females are not receptive to males for mating the first 20 hours after emergence

T. M. Perring, A. D. Cooper, C. A. Farrar, T. S. Bellows, Jr., Department of Entomology, University of California, Riverside, CA 92521.
R. J. Rodriguez, Department of Plant Pathology, University of California, Riverside, CA 92521.

*To whom correspondence should be addressed.